Resonantly absorbing one-dimensional photonic crystals

M. Artoni,[1,2] G. La Rocca,[3] and F. Bassani[3]
[1]*Department of Chemistry and Physics of Materials, University of Brescia, Italy*
[2]*European Laboratory for Non-Linear Spectroscopy, Sesto Fiorentino, Firenze, Italy*
[3]*Scuola Normale Superiore, Pisa, Italy*
(Received 5 February 2005; published 10 October 2005)

A compact theoretical description of the effects of dissipation on the propagation of light waves through a multilayer periodic mirror built from resonant absorbing atoms is presented. Depending on the lattice periodicity, ultranarrow photonic gaps, weak polaritonic gaps, as well as rather atypical gap structures may be observed. Because of the atom's absorption line shape Bloch gap modes may acquire quite a cumbersome structure which is thoroughly studied here or which may even disappear when dissipation becomes sufficiently strong. The same approach well applies also to resonantly absorbing photonic crystals based on excitonic resonances.

DOI: 10.1103/PhysRevE.72.046604 PACS number(s): 42.70.Qs, 42.50.Gy

I. INTRODUCTION

The propagation of light in complex dielectric media, namely structures with an index of refraction that has variations on a length scale that is roughly comparable to the wavelength of the incident light, is a rich and fascinating phenomenon. Such complex media strongly scatter light. In particular, if a complex material is assembled in a periodic way we obtain a crystal-like structure that under appropriate conditions may exhibit energy bands, i.e., energy regions in which light can propagate separated by regions in which light cannot propagate and hence called photonic band gaps [1,2]. Artificially engineered photonic band-gap materials are well known as *photonic crystals* [3–6]. Most of the earlier designs based on the familiar diamond like [7] or woodpile [8] structures are now being replaced with more sophisticated architectures [9,10]. The essential underlying physics is rather simple, namely constructive interference that gives rise to Bragg refraction in certain well defined directions or, in the simplest one-dimensional geometry, to Bragg reflection. Quite recent investigations, however, have also sought to discover photonic band-gap structures in natural specimens as well [11,12]. Many have existed naturally for millennia, yet the sheer physical complexity of these natural systems often renders an accurate representation of their structure extremely difficult [13].

In its simplest version, a photonic crystal is created by introducing air holes into a solid medium having a high refractive index and semiconductors certainly are most familiar instances [7]. Certain liquid crystals are also found to exhibit Bragg reflection as due to a periodicity along a specific direction of the polymer structure [14,15]. With their remarkable capabilities of localizing and guiding radiation, photonic crystals can be used to create miniature high reflectance mirrors [16], which only reflect light over the same wavelength range as the band gap, as well as narrow waveguides [17], filters [18], and microlasers [19]. They have further opened a whole new chapter in nonlinear optics [20] suggesting a conceptually new architecture for nonlinear optical materials exhibiting alternative schemes for amplification [21], for nonclassical light generation [22], enhanced photon-photon correlations [23,24], artificial anisotropy and engineered point-group symmetry [25]. Photonic crystals have finally spurred the investigation of interesting new phenomena such as superprism effects [26], negative refraction [27], negative refraction of sound waves [28], quenching of spontaneous [29] and stimulated [30] emission, refractive index enhancement [31], Lamb shift enhancement [32] and efficient control of phase matching in the generation of entangled photon pairs [33] just to mention a few. For the most part of these effects experimental demonstration has already been carried out or is under way.

One may wonder whether photonic band gaps could be observed also in spatially periodic structures made of dilute gases of resonant absorbing atoms. Unlike in a disordered gas, waves scattered from periodically ordered atoms are spatially correlated so that the coherence length for interference in directions other than the forward one will be large. When a probe beam propagates normally to a stack of thin atomic samples placed at a distance comparable to the probe wavelength and otherwise separated by vacuum, interference between forward and backward waves can strongly attenuate the incident field so as to enhance the reflected wave. Strong reflection is expected to occur over a certain range of frequencies in much the same way as that arising from the band gap of one-dimensional multilayer dielectric mirrors [34].

In the periodic dissipative atomic structures that we consider here Bragg reflection and the resulting band-gap mechanism is described through a macroscopic complex frequency-dependent dielectric function $\epsilon(\omega)$. Because the real and imaginary parts of the dielectric function are related by the Kramers-Kronig relations [35], causality implies that a medium can never be purely absorptive. A periodically modulated absorption then entails an inevitable spatial modulation of dispersion, i.e., of the index contrast required to open a band gap [34].

Although weak absorption is in general expected to affect the band structure [36–39] which one would otherwise observe in the absence of dissipation, it is not altogether clear yet what will happen in the opposite limit of substantial absorption. We anticipate that in periodic stacks made of dilute gases of resonant absorbing atoms Bloch gap modes falling near the strongly absorbing atom's resonance region may entirely disappear. A detailed analysis is here carried out for realistic ultracold atomic gas parameters.

These unusual photonic crystals may actually be created [40] either by trapping ultracold atoms in the periodic ac Stark shift potential wells of an optical lattice [41,42] or by periodically modulating absorption through electromagnetically induced transparency [43] in a standing wave pump configuration [44,45]. Notice that in this case control over the gap structure may be achieved directly through the external laser beam which creates the periodic optical potential whose lattice constant is then set with rather high precision. The second scheme, in particular, requires no spatial redistribution of the atoms [44,45]. This scheme, when compared, e.g., with band-gap control mechanisms [46] that are based on fast changes of free carriers density, becomes quite amenable to implement a new mechanism for ultrafast all-optical switching.

The photonic band structures associated with these two realistic index modulations can clearly be investigated numerically [47]. Yet we will deal here with an atomic structure which is a limiting form of what could be realized in practice, namely an array of thin atomic parallel-sided layers separated by vacuum. This will enable one to present analytical results for the propagation of electromagnetic waves through the atomic array. The main advantages of such an approach are the physical insight into the nature and significance of the photonic band gap and the ease in computing its structure. Further, such a model is particularly suited to study photonic crystals built from semiconductor structures that exhibit sharp resonantly absorbing transition lines, such as some exciton transitions [48] in cuprite (Cu_2O) or in copper cloride (CuCl).

Our results crucially depend on the optical properties of the single atomic sheet from which the periodic stack is built and these are briefly illustrated in Sec. II. In particular, the transfer matrix associated with the primitive cell of our periodic structure, whose eigenvalues are needed to determine the nature of the Bloch waves, are derived in Sec. III. The one-dimensional Bragg stack of these atomic sheets is considered in Sec. IV, where the nature of the Bloch waves can be assessed through a straightforward analytic condition. The specific structure of band-gap modes that originate from using realistic atomic parameters is thoroughly examined in this section. We discuss separately in Sec. V the possibility of band-gap tuning by modifying the laser beam configuration that creates the lattice periodicity while in Sec. VI we examine the case of gaps forming near the atom's resonance region where absorption most affects the nature of the Bloch gap modes. The main conclusions of the work are summarized in Sec. VII.

II. THE ATOMIC PERIODIC STRUCTURE

Our simplified structure takes the form of an infinite one-dimensional array of thin atomic slabs with given periodicity a. In typical experimental configurations a is set by the periodicity of the standing wave [40,45], and it is just half the wavelength of the two counter-propagating laser beams creating the optical potential. For the sake of simplicity, we will focus here on normal incidence, though the treatment could be extended to oblique incidence as well. Each slab has a thickness d sufficiently smaller than a. The effective optical thickness of the layers of atoms trapped by the optical potential is of the order of a tenth of the periodicity or less [40,45]. The optical properties of the single slab are specified by the complex dielectric function

$$\epsilon(\omega) = n^2(\omega) = \epsilon_b + 3\pi\mathcal{N}\frac{\gamma_e}{\omega_o - \omega - i\alpha\gamma_e}, \qquad (1)$$

which describes a characteristic *Lorenztian* absorption profile [35] exhibited by a probe of frequency ω impinging on a sample of two-level atoms of resonant transition frequency ω_o. Here $\epsilon_b \simeq 1$ is the sample background dielectric function while $\mathcal{N}$ is the scaled atomic average density $\lambda\!\!\!^{-}{}_o^3 N/V$ where $\lambda\!\!\!^{-} = \lambda_o/2\pi = c/\omega_o$ is the reduced resonant wavelength. For magnetically trapped ^{87}Rb atoms, e.g., the probe typically couples hyperfine components of the ground $S_{1/2}$ state with components of the excited $P_{3/2}$ state [49]. Characteristic excited level linewidth and resonant wavelength values are $\gamma_e/2\pi \simeq 6$ MHz and $\lambda_o = 780.792$ nm (D_2 line) yielding $\mathcal{N} \simeq 5.7 \times 10^{-3}$ for a typical density $N/V \simeq 3 \times 10^{12}$ cm^{-3} of rubidium at micro-kelvin temperatures.

It is here worth stressing that the dielectric function (1) also describes the $2P$ yellow exciton (line) resonant absorption in Cu_2O upon substituting [50] the decay rate $\gamma_e/2\pi$ with the $2P$ exciton linewidth $\gamma_{2P}/2\pi \simeq 242.12$ GHz, $\lambda_o \to 576.8361$ nm, and $3\pi\mathcal{N} \to |D|^2/(\epsilon_o \hbar \gamma_{2P} V) \simeq 0.02$, where $|D|^2$ is proportional to the $2P$ exciton oscillator strength. Similarly, the dielectric function (1) may also describe the Z_3-exciton resonant absorption (line) in CuCl when replacing [51] $\gamma_e/2\pi$ with the Z_3 exciton linewidth $\gamma_x/2\pi = 12.1$ GHz, $\lambda_o \to 386.9352$ nm, and $3\pi\mathcal{N} \to \epsilon_b \hbar\Delta_{LT}/\hbar\gamma_x \simeq 6.32 \times 10^2$. Here $\epsilon_b \to 5.59$ and $\hbar\Delta_{LT} = 5.65$ meV are respectively the background dielectric constant and the exciton longitudinal-transverse splitting [48]. Unlike for cuprite, which exhibits a fairly weak oscillator strength making its optical response rather similar to that of an atomic system, copper chloride has a large oscillator strength along with a narrow linewidth leading to a well developed polaritonic effect [52] which makes the response non-atom-like in nature.

Typical profiles of the real and imaginary parts of the refractive index $n(\omega) = \eta(\omega) + i\kappa(\omega)$ for rubidium atoms are shown in Fig. 1 as a function of the probe detuning $\delta = \omega_o - \omega$. Notice that the Lorentzian absorption profile can be here modified in an artificial way by a suitable scaling (α) of the damping term in the denominator of Eq. (1). While $\alpha \to 1$ corresponds to the actual linewidth profile, smaller α's yield a linewidth narrowing with a concomitant peak absorption increase [53]. The real and imaginary parts of the dielectric function $\epsilon(\omega)$ are related by the Kramers-Kronig relations and hence the scaling affects both the resonant absorption (κ) and the refractive index (η).

We will start by constructing in the next section the transfer matrix for the primitive cell of an infinite one-dimensional array of absorbing thin atomic layers with the complex index given in (1). This will then be used to derive the Bloch condition that determines the nature of the Bloch waves propagating through the array.

III. TRANSFER MATRIX

For a linearly polarized monochromatic plane wave of frequency ω and wave vector k propagating in the x direction, the electric field at an arbitrary point x,

$$\begin{aligned}\boldsymbol{E}(x,t) &= \hat{\mathbf{z}}E(x)e^{-i\omega t}\\ &= \hat{\mathbf{z}}[E^{+}(x)+E^{-}(x)]e^{-i\omega t} \equiv \hat{z}[\mathcal{E}^{+}e^{ikx}+\mathcal{E}^{-}e^{-ikx}]e^{-i\omega t}\end{aligned} \tag{2}$$

is fully determined by the two complex components $E^{+}(x)$ and $E^{-}(x)$ describing forward and backward traveling waves. If we then denote the electric field by the column vector

$$E(x) \to \begin{pmatrix} E^{+}(x) \\ E^{-}(x) \end{pmatrix} \equiv \left.\begin{pmatrix} E^{+} \\ E^{-} \end{pmatrix}\right|_{x}, \tag{3}$$

the field on the left (l) and right (r) hand side x' and x'' of a layer may in general be written as [54,55]

$$\left.\begin{pmatrix} E_r^{+} \\ E_r^{-} \end{pmatrix}\right|_{x''} = \mathcal{M} \left.\begin{pmatrix} E_l^{+} \\ E_l^{-} \end{pmatrix}\right|_{x'} \tag{4}$$

while the transformation

$$\mathcal{M} = \frac{1}{T_{rl}}\begin{pmatrix} T_{lr}T_{rl} - R_{lr}R_{rl} & R_{rl} \\ -R_{lr} & 1 \end{pmatrix} \tag{5}$$

can be expressed [56] in terms of the reflection and transmission complex amplitudes for a *forward* (R_{lr}, T_{lr}) and *backward* (R_{lr}, T_{lr}) propagating wave. For a layer of thickness d, whose boundaries separate three media of refractive index n_1, n_2, and n_3, the reflection and transmission amplitudes for the forward and backward wave are, respectively,

$$R_{13} = \frac{r_{12} + r_{23}e^{2ikdn_2}}{1 + r_{12}r_{23}e^{2ikdn_2}} \quad T_{13} = \frac{t_{12}t_{23}e^{ikdn_2}}{1 + r_{12}r_{23}e^{2ikdn_2}}, \tag{6}$$

and

$$R_{31} = -\frac{r_{23} + r_{12}e^{2ikdn_2}}{1 + r_{12}r_{23}e^{2ikdn_2}} \quad T_{31} = \frac{t_{32}t_{21}e^{ikdn_2}}{1 + r_{12}r_{23}e^{2ikdn_2}}. \tag{7}$$

The normal incidence Fresnel coefficients r_{12}, t_{12}, r_{23}, and t_{23} as well as t_{32} and t_{21} on the two interfaces of the layer [57] are evaluated at the incident wave frequency $\omega = ck$ which is omitted here. In particular, when $n_1 = n_3 = 1$ and one has $R_{31} = R_{13}$ Eq. (4) becomes

$$\left.\begin{pmatrix} E_3^{+} \\ E_3^{-} \end{pmatrix}\right|_{x+d} = \mathcal{M} \left.\begin{pmatrix} E_1^{+} \\ E_1^{-} \end{pmatrix}\right|_{x} \tag{8}$$

with

$$\mathcal{M} = \frac{1}{4n_2}\begin{pmatrix} (n_2+1)^2e^{ikdn_2} - (n_2-1)^2e^{-ikdn_2} & (n_2^2-1)e^{ikdn_2} - (n_2^2-1)e^{-ikdn_2} \\ (n_2^2-1)e^{-ikdn_2} - (n_2^2-1)e^{ikdn_2} & (n_2+1)^2e^{-ikdn_2} - (n_2-1)^2e^{ikdn_2} \end{pmatrix}. \tag{9}$$

The relation (8) holds for a generic absorbing and dispersive medium and hence $\mathcal{M}$ constitutes the most general expression for the *transfer matrix* of a homogeneous optical layer of thickness d and complex refractive index $n_2(\omega)$. This will be used in the following sections.

IV. BLOCH MODES

We proceed to examine the structure of the photonic Bloch modes by studying the propagation of electromagnetic waves across an *infinite* one-dimensional array of thin atomic layers with optical properties specified by the complex dielectric function (1) and otherwise separated by vacuum. The layers spatial arrangement is shown in Fig. 2.

For a linearly polarized wave propagating along the x direction across the array, the electric field $\boldsymbol{E}_n$ in the free space region between the barriers labeled by $n-1$ and n can be written as in (2) in terms of its amplitude $\mathcal{E}_n^{\pm}$ and space-dependent phase components in the form

$$\begin{aligned}\boldsymbol{E}_n(x,t) &= \hat{z}[E_n^{+}(x)+E_n^{-}(x)]e^{-i\omega t}\\ &= \hat{z}[\mathcal{E}_n^{+}e^{ikx}+\mathcal{E}_n^{-}e^{-ikx}]e^{-i\omega t},\end{aligned} \tag{10}$$

where ω and $k = \omega/c$ are, respectively, the frequency and wavevector of the *local* propagating modes as determined by the incident field. The relations between the fields in adjacent primitive cells can be obtained by application of the boundary conditions at the dielectric interfaces [35,56]. According to (8) the resulting relation between the electric fields in cells n and $n+1$ is conveniently written in matrix notation as

$$\left.\begin{pmatrix} E_{n+1}^{+} \\ E_{n+1}^{-} \end{pmatrix}\right|_{x=na+(d/2)} = \mathcal{M} \left.\begin{pmatrix} E_n^{+} \\ E_n^{-} \end{pmatrix}\right|_{x=na-(d/2)}, \tag{11}$$

where the electric fields $E^{\pm}$ are to be evaluated at the values indicated in the equation and where $\mathcal{M}$ is the transfer matrix (9) with $n_2(\omega) \to n(\omega)$ as given in (1). The relation between the electric fields at the borders of the nth cell free space region, on the other hand, is obtained directly with the help of (10) and can be cast again in the matrix form

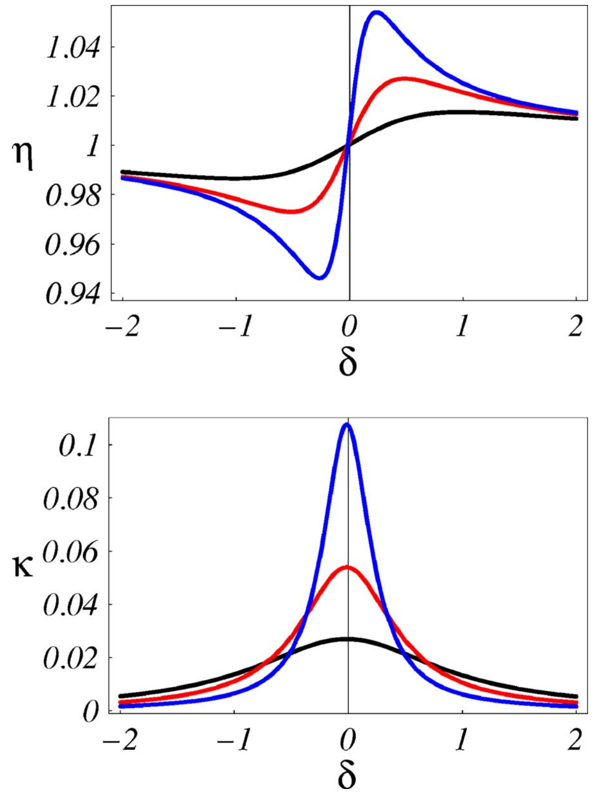

FIG. 1. (Color online) Real (η) and imaginary (κ) parts of the single layer refractive index in (1) for ultracold ^{87}Rb atoms with a density $N/V=3\times10^{12}$ cm^{-3}. The probe detuning δ is in units of the excited state decay rate γ_e. The different curves correspond to different absorption line shape scale factors with $\alpha=0.25$ (blue), $\alpha=0.5$ (red) and with $\alpha=1$ (black) corresponding to actual absorption Lorentzian linewidth profile.

$$\begin{pmatrix} E^+_{n+1} \\ E^-_{n+1} \end{pmatrix}\Bigg|_{x=(n+1)a-(d/2)} = \begin{pmatrix} e^{i\mathscr{k}(a-d)} & 0 \\ 0 & e^{-i\mathscr{k}(a-d)} \end{pmatrix},$$

$$\begin{pmatrix} E^+_{n+1} \\ E^-_{n+1} \end{pmatrix}\Bigg|_{x=na+(d/2)} \equiv M \begin{pmatrix} E^+_{n} \\ E^-_{n} \end{pmatrix}\Bigg|_{x=na-(d/2)}, \tag{12}$$

where

$$M = \begin{pmatrix} e^{i\mathscr{k}(a-d)} & 0 \\ 0 & e^{-i\mathscr{k}(a-d)} \end{pmatrix}\mathcal{M} \tag{13}$$

is the primitive cell transfer matrix, with $\det M=1$.

The relation between the electric-field given in (11) and (12) are entirely derived from the properties of the electromagnetic field but these same fields are independently related by Bloch's theorem [58], which applies generally to all forms of excitation in a periodic structure. For the present configuration, Bloch's theorem takes the form

$$E_{n+1}(x+a) = e^{ika}E_n(x) \tag{14}$$

or

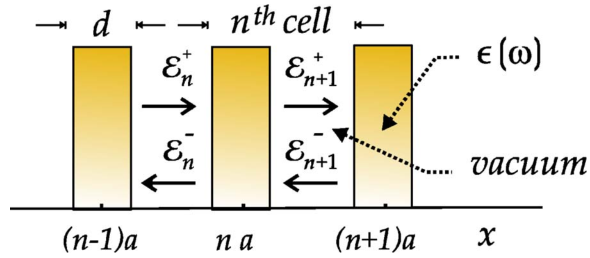

FIG. 2. (Color online) Geometrical arrangement of the one-dimensional array of atomic layers with periodicity a. Each primitive cell comprises a layer of thickness $d=a/20$ described by a complex dielectric function $\epsilon(\omega)$ and vacuum while $\mathcal{E}^{\pm}$ describes the local electric field amplitudes.

$$\begin{pmatrix} E^+_{n+1} \\ E^-_{n+1} \end{pmatrix}\Bigg|_{x=(n+1)a-(d/2)} = \begin{pmatrix} e^{ika} & 0 \\ 0 & e^{ika} \end{pmatrix}\begin{pmatrix} E^+_{n} \\ E^-_{n} \end{pmatrix}\Bigg|_{x=na-(d/2)}, \tag{15}$$

with the same notation for $E^{\pm}$ as used in Eqs. (11) and (12). Combining now Eq. (12) with Eq. (15) yields

$$\left[M - \begin{pmatrix} e^{ika} & 0 \\ 0 & e^{ika} \end{pmatrix}\right]\begin{pmatrix} E^+_{n} \\ E^-_{n} \end{pmatrix}\Bigg|_{x=na-(d/2)} = 0. \tag{16}$$

Note that the one-dimensional *Bloch wave vector* k, which is complex in general, determines the spatial development of the phase of the photonic excitation as it propagates through the periodic medium. Equation (16) identifies the Bloch exponent e^{ika} as the eigenvalue of the primitive cell transfer matrix M, and the corresponding determinant equation requires that

$$e^{2ika} - \mathrm{Tr}(M)e^{ika} + 1 = 0. \tag{17}$$

If k is a solution also $-k$ is a solution, and hence

$$e^{ika} + e^{-ika} = \mathrm{Tr}(M) \equiv \beta(\omega) \tag{18}$$

with

$$\beta(\omega) = (e^{in\omega d/c} + e^{-in\omega d/c})\cos \omega(a-d)/c + i\frac{n^2+1}{2n}(e^{in\omega d/c} - e^{-in\omega d/c})\sin \omega(a-d)/c. \tag{19}$$

Here the incident wave vector $\mathscr{k}$ has been replaced by ω/c while the index frequency dependence is again omitted.

Solutions of Eq. (18) determine the dispersion of the Bloch modes, i.e., the dependence of the complex Bloch wave vector $k\equiv k'+ik''$ on the frequency ω of the incident wave. It can be seen directly from (19) that for a transparent medium with a *real* refractive index $\beta(\omega)$ becomes real. The frequency region where $|\beta(\omega)|\leq 2$ correspond to the allowed bands with k real. The region where $|\beta(\omega)|>2$ corresponds instead to the forbidden gaps where k acquires an imaginary part and, at the same time, its real part is either 0 or $\pm\pi/a$ for gaps lying, respectively, at the center or at the boundaries of the first Brillouin zone. Such restriction directly follows from the fact that for real β one has $\sin k'a=0$ [55] when $k''\neq 0$. In the limiting case of a uniform atomic medium ($d\rightarrow a$)

with a *real* refractive index, $\beta(\omega)\rightarrow\cos(\omega na/c)$ and (18) yields

$$k = k' = \pm n\frac{\omega}{c} \quad \left(\mathrm{mod}\ \frac{2\pi}{a}\right). \tag{20}$$

This recovers the well known photon dispersion, folded back into the first Brillouin zone

$$-\frac{\pi}{a} \leqslant k' \leqslant \frac{\pi}{a}, \tag{21}$$

or the photon vacuum dispersion when $n\rightarrow 1$. For an array of atomic layers $(d\neq a)$ exhibiting strong absorption $\beta(\omega)$ is instead a rather involved complex function and the complex Bloch vector k associated with a given incident frequency ω can be obtained as a solution of the equation of complex argument

$$ka = \pm\cos^{-1}\left[\frac{\beta(\omega)}{2}\right] \quad (\mathrm{mod}\ 2\pi), \tag{22}$$

with k' folded back into the first Brillouin zone.

In a *nondissipative* periodic medium solutions of (22) are characterized by a real frequency ω yielding the band structure with allowed frequency zones separated by forbidden gaps. If ω falls inside an allowed band the Bloch vector k is a real solution of (22), but k acquires instead an imaginary part when ω falls inside the gap. While the former solutions describe light waves that propagate in the medium, the latter ones can be interpreted as surface excitations (*Tamm states*). In a bounded medium these are evanescent waves that undergo *extinction* inside the medium in the direction normal to the boundary [59] and hence do not represent propagating modes. The decay is due to strong Bragg reflections, a reversible process which does not lead to transfer of energy to the medium making then reflection within the gap strictly unity. Such an extinction process only occurs within the band gap while $k''\rightarrow 0$ for all other modes.

In a *dissipative* periodic medium the situation becomes rather intricate. The non-vanishing imaginary part of the refractive index $n(\omega)$ causes now *absorption* and ω and k solutions of (22) are, in general, complex. These solutions can be cast, for instance, either in the form $\omega=\omega'+i\omega''$ with real k or in the form $k=k'+ik''$ with real ω. Because in a bounded medium the Bloch waves, excited by the incident field at a given real frequency ω, decays exponentially with the distance from the sample boundary the latter representation is more appropriate to describe spatial decay of the Bloch modes studied here. In an absorbing periodic medium propagation of Bloch waves is damped; this is a dissipative process in which energy is transferred to the medium and generally prevents reflection from being unity. Unlike for the extinction process, absorption entails that $k''\neq 0$ even for modes ω falling within an allowed band. In turn, within a forbidden gap k' is no longer restricted to be exactly 0 or π/a and hence the distinction between allowed band and forbidden gaps becomes fairly blurred [36,39]. Dissipation, as a matter of fact, modifies the band-gap structure which one would observe in the absence of absorption. For large degrees of dissipation the band gap may even disappear, a rather important issue which we discuss separately in Sec. VI.

Figure 3 show the solutions of Eq. (22) for an infinite stack of atomic layers around the X point of the first Brillouin zone [60]. The wave vector components k' and k'' are plotted here against the incident probe beam frequency detuning from the atom's resonance ω_o and two separate forbidden gaps are seen to open for certain ranges of frequencies below $(\delta>0)$ and above $(\delta<0)$ resonance. Frequencies ω, for which $k'a=\pi$ and $k''a\neq 0$, characterize *photonic band-gap* modes at the Brillouin zone boundary.

As we may in general express $k'=\omega\tilde{\eta}(\omega)/c$ in terms of an *effective* refractive index $\tilde{\eta}$ for the array [61], an estimate for the midgap frequencies ω_g may be obtained from solving the equation

$$\omega_g\tilde{\eta}(\omega_g) = \frac{\pi}{a}c. \tag{23}$$

In particular, when the resonant frequency ω_o falls sufficiently close to the Bragg frequency [62], the incident and reflected photon modes generally mix with the resonance mode as in Fig. 3. Such a mixing causes the two photon modes to repel with subsequent splitting of the gap while Eq. (23) exhibits three distinct solutions, two of which are physical solutions representing the centers of the two split gaps.

The gap region above resonance on the left has sharp edges and a mode extinction profile which is symmetric around midgap as for a traditional nondissipative photonic band-gap [3,4]. In this case, in fact, the gap modes all fall far from resonance making the atomic periodic structure essentially nondissipative. It is to be noted that k'' is *negative* within this gap and around its upper edge (*second band*) as in this spectral region the corresponding k' is obtained by folding into the first Brillouin zone solutions for which $k'\leqslant-\pi/a$. In general, the correct sign of k'' is the one ensuring that damping occurs in the direction of energy propagation as determined, for weak absorption [63,64], by the usual group velocity $v_g^{-1}=\partial k'/\partial\omega$. This entails that below the lower edge of the gap (*first band*) k'' should be positive as the group velocity changes from positive to negative across the gap. The two distinct k'' matchings at the borders of the gap are clearly shown in the insets of Fig. 3(b).

Conversely, the other gap on the right lies next to the resonance region where dissipation is strong instead. Absorption makes the mode extinction profile no longer symmetric and much more pronounced. The characteristic sharp spike observed at resonance, in particular, is due to resonant absorption. This is clearly shown in Fig. 3(d) where the region is resolved on a much larger scale. We plot here the Bloch wavevector for the three different absorption profiles of Fig. 1 to examine the band edge modifications associated with different absorption profiles. In all three cases k'' is positive inside the gap and remains positive across the lower edge consistently with the fact that the group velocity is positive there, while k'' flips sign across the upper edge where the group velocity becomes negative next to the resonance region where absorption is still small. For the case in which $\alpha\rightarrow 1$, however, the group velocity becomes negative but

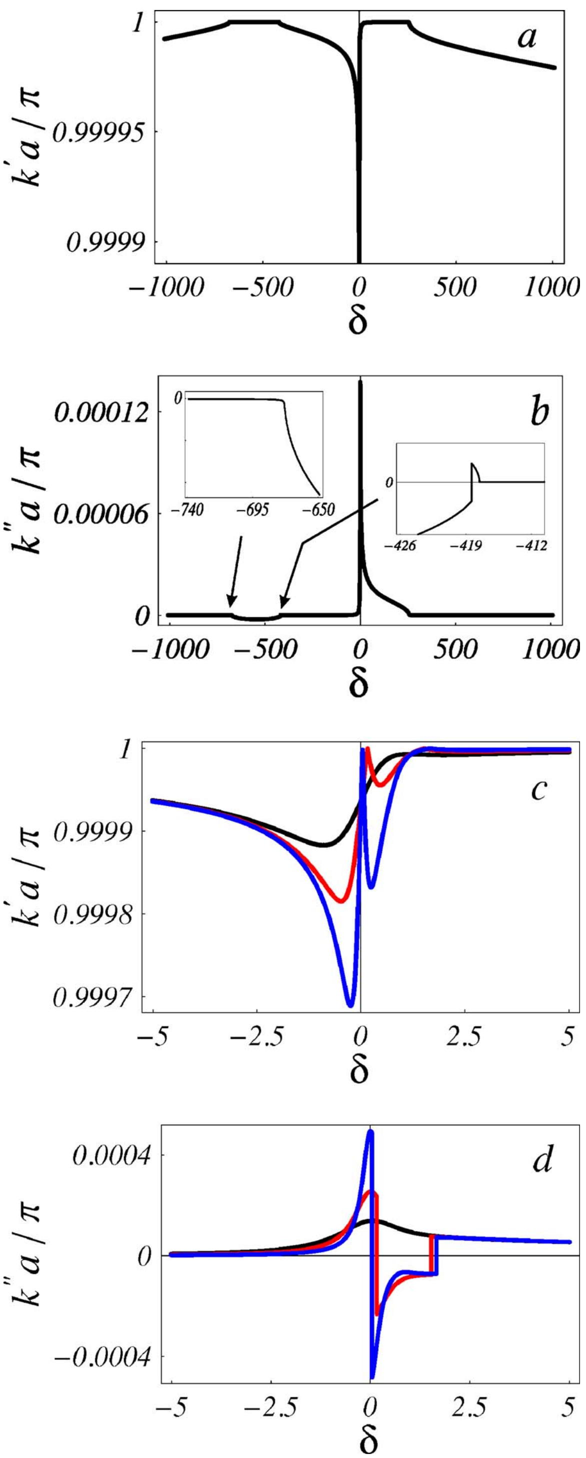

FIG. 3. (Color online) Real (a) and imaginary (b) Bloch wave vector scaled components as a function of the probe detuning for an atomic stack with periodicity $a \simeq 390.393$ nm and layers of thickness $d=a/20$. All other atomic parameters are as in Fig. 1. A band gap appears at the edge of the first Brillouin zone $k'=\pi/a$ and is not continuous. Away from the gap the dispersion becomes linear. The steep profile for blue detunings is due to resonance absorption. Real (c) and imaginary (d) parts of the Bloch vector k in the resonance region for the three different absorption profiles of Fig. 1 with $\alpha=0.25$ (blue), $\alpha=0.5$ (red), and $\alpha=1$ (black). Near resonance the edge of the gap is slightly modified depending on the absorption profile.

unlike the previous case k'' remains positive. This occurs in a region where absorption is, however, large and where the group velocity loses its physical significance [64]. Merging of the absorption and extinction regimes takes place around a typical atomic linewidth (γ_e) below resonance [Fig. 3(d)] with a concomitant shift of the edge of the gap depending on the absorption profile [Fig. 3(c)]. Figures 3(c) and 3(d) show the different propagating nature of the Bloch modes within the resonance region where propagating modes with increasing absorption ($|\delta| \lesssim \gamma_e$) combine with band-gap modes with an appreciable degree of extinction ($\delta > \gamma_e$).

The above results and discussion all refer to Bloch modes in a *perfect* and *infinite* periodic stack of parallel-sided layers of atoms. Because of atomic fluctuations the layers width (d) and periodicity (a) will not remain accurately fixed under realistic experimental conditions yet, in general, this will not modify appreciably the band-gap structure [65]. Typical experimental investigations, on the other hand, focus [3,4,6] on the transmission and reflection of electromagnetic waves through samples of finite length. Even with the knowledge of the photonic band structure as calculated above for an infinite stack, drawing a meaningful comparison with measured transmission and reflection spectra is still a nontrivial task. The two gaps may not yield indeed the same transmission patterns owing to the different extinction per unit length values they exhibit. As discussed above the number of primitive cells may be in fact sufficient to contain the evanescent modes that extinguish within one of the gaps though it may not for the other.

It is then necessary to consider a *finite* sample of thickness $L=Na$ where N is the number of primitive cells or *periods* the stack is made of. The transfer matrix approach is ideally suited for this situation as one may introduce the entire stack transfer matrix in terms of the primitive cell matrix M in Eq. (13) simply as $M_N=M^N$. Because $\det M=1$, it can be shown that the following closed expression for M_N holds true [56]

$$M_N = \frac{\sin Nka}{\sin ka} M - \frac{\sin(N-1)ka}{\sin ka} \mathbf{1}, \tag{24}$$

where $\mathbf{1}$ is the unity matrix. Such a compact expression enables one to write the reflection (R_N) and transmission (T_N) amplitudes for an N periods stack in terms of the complex Bloch wave vector k and the elements m_{ij} of the matrix M, namely,

$$R_N = \frac{M_{N(12)}}{M_{N(22)}} = \frac{m_{12}\sin(kaN)}{m_{22}\sin(kaN) - \sin[ka(N-1)]}, \tag{25}$$

$$T_N = \frac{1}{M_{N(22)}} = \frac{\sin(ka)}{m_{22}\sin(kaN) - \sin[ka(N-1)]}, \tag{26}$$

from which, in turn, the reflectivity, transmissivity and absorption can be readily found by calculating, respectively, $|R_N|^2$, $|T_N|^2$ and $A=1-|R_N|^2-|T_N|^2$.

The reflectivity for atomic stacks of different lengths is plotted in Fig. 4. It is clear upon comparing Fig. 3(a) and Fig. 4(a) that the two gaps that one expects to appear above and below resonance may only be observed for the *thicker*

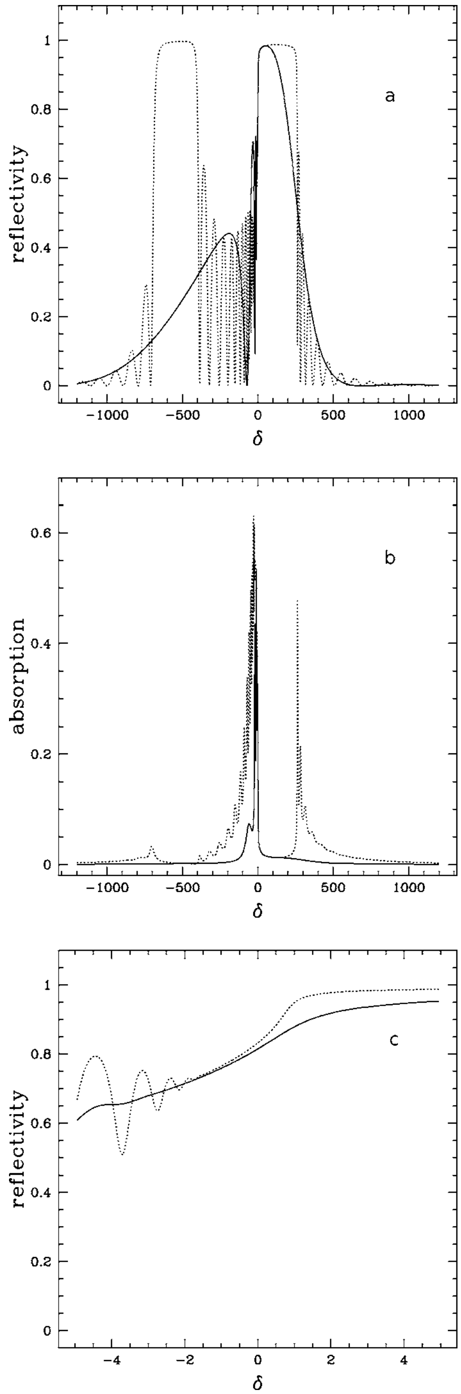

FIG. 4. Band-gap reflectivity (a) and absorption (b) profiles for the region shown in Fig. 3 when an array of length $L=6.5\times 10^4 a$ (solid) and $L=5.25\times 10^5 a$ (dotted) is used. For trapped ^{87}Rb [49] atoms L turns out to be about 2.5 cm for the shortest atomic stack. Resonance region blowup (c) for the shortest stack and different absorption profiles with $\alpha=1$ (solid) and $\alpha=0.25$ (dashed).

sample whose length (L) indeed exceeds typical values of the extinction (l_{ext}) and absorption (l_{abs}) length. The latter may easily be inferred [66] from Fig. 3(b) where right at resonance one has $l_{abs}\simeq 1.5\times 10^3 a$ while moving below resonance and outside the absorption bandwidth, when the extinction process dominates over absorption, one has $l_{ext}\simeq 7\times 10^4 a$ around midgap. Appreciably larger extinctions are observed instead in the gap above resonance where one has $l_{ext}\simeq 5\times 10^5 a$, which is just about the length of the longer stack in Fig. 4(a). For the *shorter* sample instead large reflection occurs only for the gap below resonance on the right. Owing to the increasingly smaller values of the extinction as one recedes away from resonance, reflection becomes smaller and smaller which results into a rather narrow gap. At frequencies around midgap, e.g., l_{ext} is just about the shorter sample length. On the other hand, for the range of frequencies where a gap is expected to appear above resonance in Fig. 3, extinction lengths are always too large for a strong reflection to build preventing then a well developed photonic band gap to form. For intermediate values of the length, not shown here, the broad reflection peak above resonance shifts and sharpens, merging into the well developed gap shown on the left of Fig. 4 (upper).

Figure 4 also exhibits characteristic Fabry-Pérot fringes [56] that form around the gap band-edges where interference is strongest. The frequency spacing between peaks, which increases as we move away from the edge, is directly related to departures of the photon dispersion from linear. Different spacings correspond indeed to different local slopes of the dispersion around the band edges, as clearly shown in Fig. 3(a). Such fringes, which depend on the atomic sample size, are seen to degrade with absorption. For periodic structures made of dilute gases of resonant absorbing atoms the fringe structure is then rather fragile unless weakly absorbing samples are used [cf. Fig. 4 (lower)].

V. BAND-GAP TUNING

The photonic band-gap structure discussed in the previous section may however be easily modified. In common experimental configurations this may be achieved mainly by acting on the interfering laser beams that determine the optical potential periodicity a. For one-dimensional lattices this is most effectively done [67–69] by misaligning the two beams creating the potential.

An example is shown in Fig. 5 where a slight misalignment [71] is sufficient to modify the photonic band gap of Fig. 3 into a broader one with a smaller *hole* and placed on the opposite side of resonance. Notice that the two gaps around the hole [Fig. 5(a)] are wider than the ones observed in Fig. 3(a). This originates from the resonant enhancement of the index η which, as shown in Fig. 1, undergoes a few percents increase around resonance improving the index contrast responsible for the widening of the gaps. The two portions of the split gap exhibit quite different degrees of extinction (l_{ext}) while different extinctions occur also within the same gap [Fig. 5(b)]. For mid-gap modes above and below resonance the corresponding lengths l_{ext}^L and l_{ext}^R vary from few to several cm's while only moving toward resonance l_{ext}^L falls below a cm in length. We also show in Figs. 5(c) and 5(d) a blowup of the resonance region displaying a behavior similar to that observed in Figs. 3(c) and 3(d) which one can then discuss in the same manner. Notice that parameters may also be chosen so as to obtain as done in Fig. 6 a traditional photonic band gap that splits right around resonance.

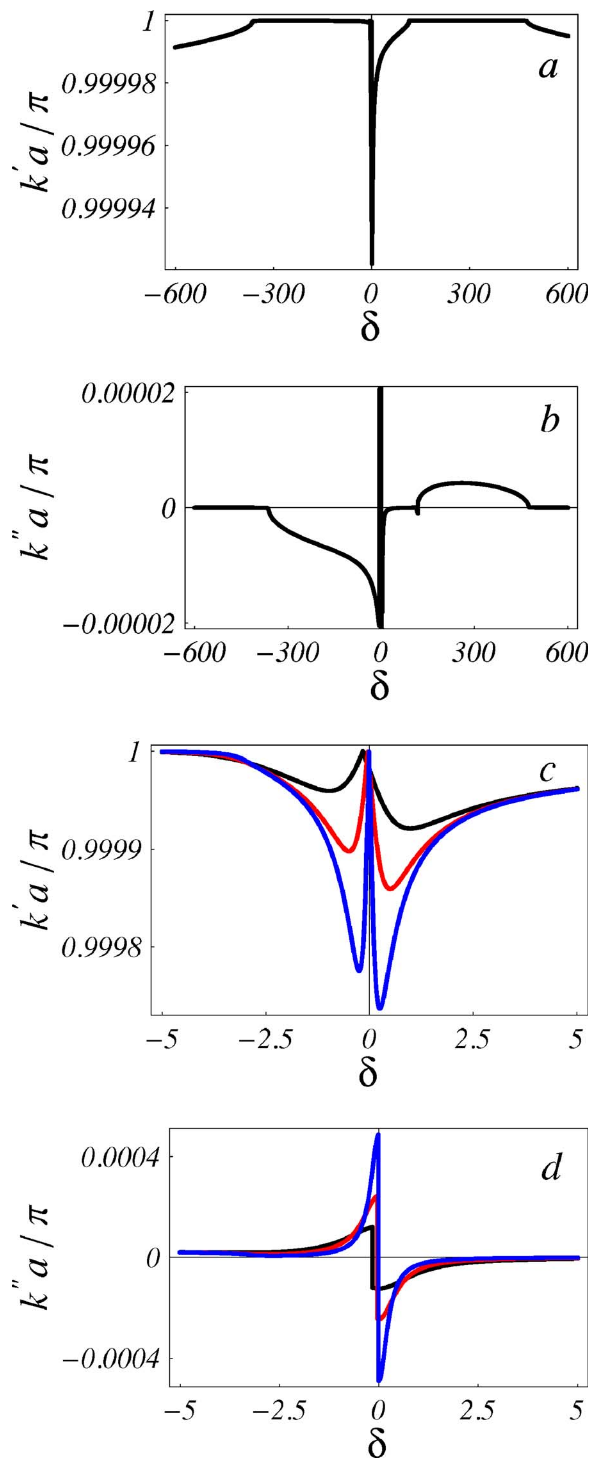

FIG. 5. (Color online) Photonic band profiles (a), (b) and resonance region blowup (c), (d) for a stack with periodicity $a \simeq 390.397$ nm. All other parameters are as in Fig. 3. Splitting of the gap occurs now below resonance.

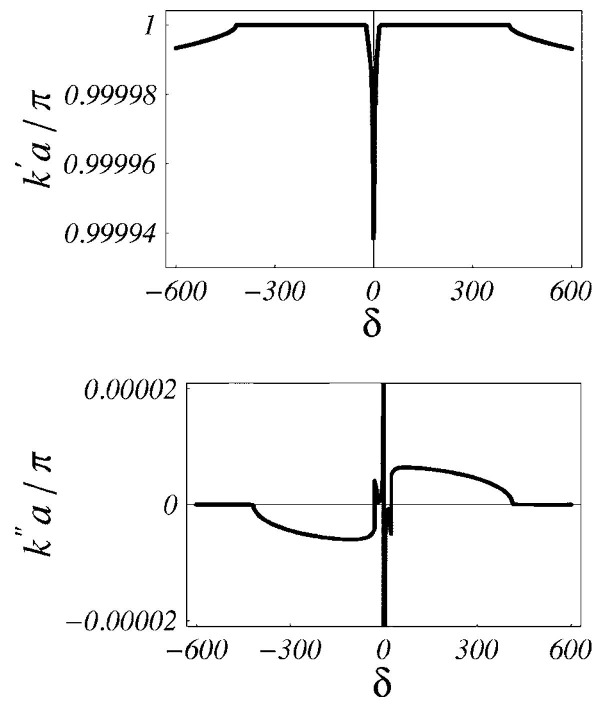

FIG. 6. Symmetric band-gap splitting obtained from an atomic stack with periodicity $a \simeq 390.396$ nm. All other parameters are as in Fig. 3. Both profiles appear to be symmetric with respect to resonance with two solutions of Eq. (23) falling at $\delta_B = \omega_o - \omega_B \simeq \pm 260$.

Unlike for solid dielectric media [3,4], the gap widths for the dilute atomic samples considered here turn out to be extremely narrow and on the GHz range. This arises from the fact that most of the gap stretches over incident frequencies that lie very much off resonance where dispersion is essentially absent, making the refractive index contrast rather small. The atomic layer thickness is also much smaller than the length of the elementary cell $(d \ll a)$ which further contributes to make the scattering strength of the optical lattice rather small. The strength may clearly depend also on the sample optical density and it can be shown that ten times as much wide gaps can be attained at the characteristic higher densities of Bose-Einstein condensed atomic gases [72].

VI. DISSIPATION AND BLOCH MODES

The scattering strength increases considerably also near an absorbing resonance. Yet it is not altogether apparent [39] how the structure of gaps developing in a strong dissipative regime would be modified. Such modifications are most conspicuous for gaps that develop [73] as in Figs. 7 and 8 within the atom's resonance region. Unlike in the examples examined in the previous two sections, the gap centered at nearly half γ_e above resonance is quite weak (Fig. 8 *black*) while absorption seems to alter in a drastic way the structure of the Bloch gap modes (Fig. 7 *black*). All modes, in fact, are allowed $(k'a \neq \pi)$ but damped $(k'' \neq 0)$ and a gap hardly develops. The incident energy is in this case mostly absorbed into the medium making reflection quite small across the resonance region as clearly shown in Fig. 8 (*black*). The tiny reflection would then make the observation of the gap position, typically done through reflection rate measurements, rather unlikely.

These results should be compared with those obtained using narrower absorption profiles. A well developed gap ap-

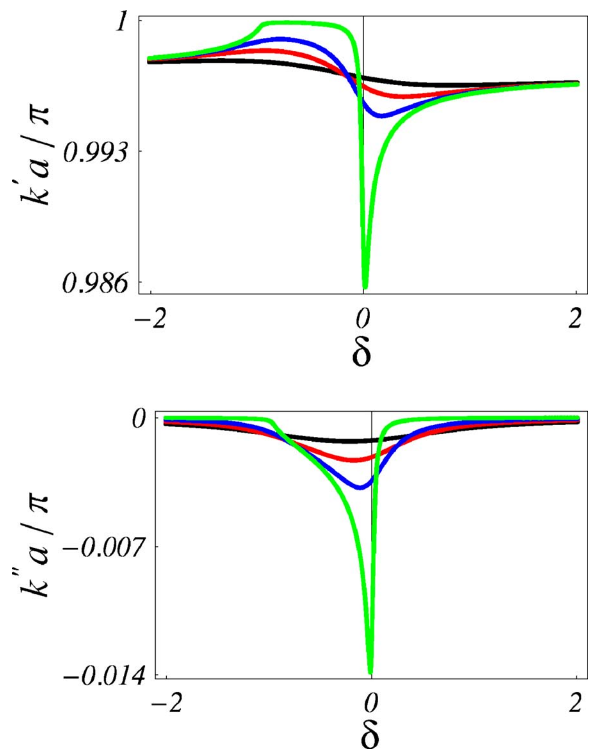

FIG. 7. (Color online) Scaled Bloch wave vector components for a stack of atomic layers of rubidium. The periodicity is $a \simeq 391.490$ nm with layers of thickness $d=a/20$, while the different absorption profiles correspond to $\alpha=0.025$ (green), $\alpha=0.25$ (blue), $\alpha=0.5$ (red), and $\alpha=1$ (black). The gap only survives for narrow absorption bandwidths.

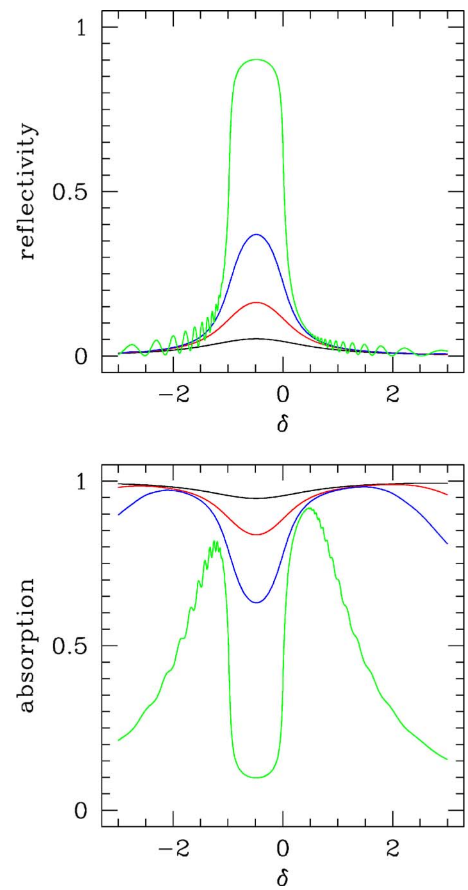

FIG. 8. (Color online) Gap reflectivity and absorption profiles for the region shown in Fig. 7 when an array of length $L=8.2 \times 10^3 a$ is used.

pears for the smallest bandwidth (*green*), while propagation is allowed outside the gap with negligible damping ($k'' \approx 0$). As the absorption profile (κ) broadens (*blue*) the gap shrinks and propagation damps around the band edges that one would observe in the nearly absence of absorption. When the absorption bandwidth increases further (*red*) propagation starts to become no longer forbidden ($k'a < \pi$) with a concomitant shift from the extinction to the absorption regime.

Figure 8, in addition, shows that the gap mechanism remains efficient only for appropriate sample lengths. For frequencies falling around the midgap (*blue*), the fraction of light which is not reflected is almost completely absorbed [66] over lengths of 400 periods or more while for the actual profile (*black*) the absorption length increases to approximately 900 periods. For trapped ^{87}Rb atoms [49] this would clearly set the smallest sample size to be not less than 160 μm in one case and nearly 350 μm in the other.

It is also worthwhile noting that in a narrow frequency range above resonance, yet outside both the atom's absorption bandwidth and the forbidden gap region (*green*), the group velocity is positive while remaining $k'' < 0$. Because all modes here arise from propagation in the region $k' \leqslant -\pi/a$ this seems to indicate that damping and propagation of electromagnetic energy take place in opposite directions. Such an apparent amplification would however bear essentially no meaning owing to the very large group velocity dispersion that a light pulse would experience over such a narrow frequency range.

The above comparison of different absorption widths sheds light into the nature of the Bloch modes that develop within the strongly absorptive atom's resonance region. Due to the resonant nature of absorption, in fact, a *polariton* dispersion [52] rather than a purely photon dispersion is relevant here. For the narrower profile (*green*) a gap is fully developed whose width is simply determined by the separation between the upper polariton branch evaluated at the edge ($k=\pi/a$) of the first Brillouin zone and the resonant frequency ω_o. The resulting gap (*green*) in Fig. 7 arises then from a typical polaritonic effect and hence resembles much more to a polariton-stop band [52] rather than to a photonic band gap. When the linewidth or oscillator strength ratio given by $\alpha/(3\pi\mathcal{N})$ increases, polaritonic effects are washed out. For the largest linewidth (*black*), in fact, the Bloch dispersion around resonance nearly flattens down to that of a photon with a tiny absorption dip (Fig. 7).

To support the above interpretation we report in Fig. 9 the modes structure around the X point for an infinite stack of CuCl layers. Cupper cloride is a prototype example of semiconductor having an allowed interband transition, pronounced exciton resonances [48] with a fully developed Z_3-exciton polaritonic stop band. The mode dispersion in Fig. 9 is obtained by using a complex dielectric function [51] similar to that used in (1) and where the relevant parameters are given in Sec. II. The oscillator strength is now four or-

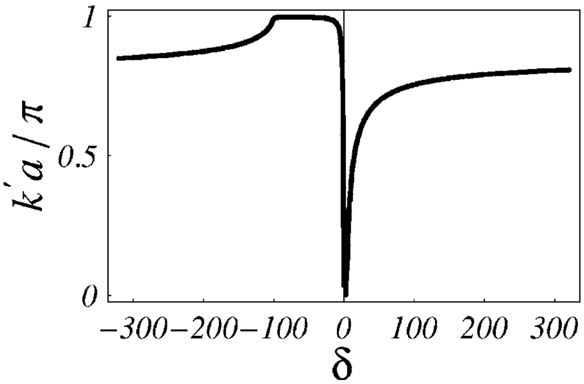

FIG. 9. Scaled Bloch real wave vector component as a function of the probe detuning for a periodic stack of CuCl layers. The periodicity is $a=210$ nm with layers of thickness $d=a/20$. The detuning δ is in units of the Z_3 exciton decay rate $\hbar\gamma_x=50$ μeV.

ders of magnitude larger than the one used for cold Rb atoms in Fig. 7 leading to a very small ratio $\alpha/(3\pi\mathcal{N})$ which gives rise to a well developed polaritonic stop band even for a unity value of α.

Again, note that unlike in the cases examined in the previous sections the stack's Bragg frequency ω_B falls far from resonance [62]. The profile shown in Fig. 7 lies in fact within the second (photonic) band above ω_B and hence the characteristic split-gap structure observed in Fig. 3, caused by the fact that ω_B and ω_o are sufficiently close to one another, does not occur here.

VII. CONCLUDING REMARKS

We have employed a straightforward approach to study the propagation of electromagnetic waves through a one-dimensional model of a periodic lattice of ultracold resonant absorbing atoms. The model provides a simplified yet sound physical picture of the photonic band structure in such lattices. The explicit formulation laid down in Sec. IV specially lends itself to assess effects of dissipation on the nature of Bloch waves in these lattices and the straightforward analytic condition (18), in particular, is here used to assess the effect of dissipation on the structure of Bloch gap modes.

Depending on the position of the atomic lattice Bragg's frequency with respect to the atom's resonance, both photonic and polaritonic gaps or rather singular gap structures may appear. While a photonic gap originates from multiple photon scattering by spatially correlated scatterers, polaritonic gaps arise instead from the photon coupling with elementary excitations such as atomic, excitonic or optical phonon resonances in the medium. In realistic periodic stacks of ultracold resonant absorbing atoms [41,45] these diverse gap structures could easily be accessed by controlling the geometrical configuration of the external optical potential which confines the cloud of ultracold atoms [69,70].

In general, absorption is seen to affect the structure of a gap which one would instead observe for an ideally nondissipative periodic lattice. In the limit of *weak dissipation* our results recover earlier theoretical work on weakly dissipative one-dimensional periodic structures [36], where weak absorption was introduced through a perturbative expansion in the imaginary part of a generic dielectric function $\epsilon(\omega)$. In the appropriate limit of infinitesimal atomic sheets, on the other hand, some of our results recover those for one-dimensional band gaps originating from an array of δ-function potentials as studied in [41]. Our treatment is however general, is not restricted to small absorption and is based on a more realistic arrangement of alternating thin parallel sided layers, and hence also amenable to photonic crystals built from absorbing dielectric or semiconducting materials.

Bloch gap modes do not generally survive in the presence of strong dissipation and to illustrate this point further we have thoroughly examined realistic periodic atomic stacks whose band gaps develop either entirely or only in part within the absorbing region of the atom's Lorentzian absorption line shape.

ACKNOWLEDGMENTS

We would like to thank R. Sapienza, J. Bertolotti, S. Gottardo, J. Carusotto, V. Agranovich, L. Andreani, C. Deone, and M. Inguscio for fruitful discussions. We acknowledge financial support from the EU (Contract HPRICT1999-00111) and M.I.U.R. (Prin 2002-28858 and Actione Integrada Italia-Spagna IT-1603).

[1] E. Yablonovitch, Phys. Rev. Lett. **58**, 2059 (1987).
[2] S. John, Phys. Rev. Lett. **58**, 2486 (1987).
[3] J. Joannopoulos, R. Meade, and J. Winn, *Photonic Crystals: Moulding the Flow of Light* (Princeton University Press, Princeton, NJ, 1995).
[4] K. Sakoda, *Optical Properties of Photonic Crystals* (Springer, Berlin, 2001).
[5] S. Johnson, J. Joannopoulos, R. Meade, and J. Winn, *Photonic Crystals: The Road from Theory to Practice* (Kluwer, Norwell, 2002).
[6] D. Wiersma *et al.*, in *Waves Scattering in Complex Media: from Theory to Applications* (Kluwer, Dordrecht, 2003).
[7] K. M. Ho, C. T. Chan, and C. M. Soukoulis, Phys. Rev. Lett. **65**, 3152 (1990); O. Toader and S. John, Phys. Rev. E **66**, 016610 (2002).
[8] For woodpile structures that exhibit band gaps in the microwaves, infrared, and visible range see, e.g., S. Y. Lin *et al.*, Nature (London) **394**, 251 (1998) (microwaves); E. Ozbay *et al.*, Phys. Rev. B **50**, 1945 (1994) (infrared); and M. J. A. de Dood *et al.*, Phys. Rev. B **67**, 035322 (2003) (visible).
[9] O. Toader *et al.*, Science **292**, 1133 (2001).
[10] E. Yablonovitch, Nat. Mater. **2**, 648 (2003).
[11] A. Parker, Proc. R. Soc. London, Ser. B **265**, 967 (1998).
[12] P. Vukusic *et al.*, Nature (London) **424**, 852 (2003).
[13] Only recently rigorous modeling of such natural structures has begun to address some aspects of these complex structures. See, e.g., B. Gralak *et al.*, Opt. Express **9**, 567 (2001).
[14] G. Abbate *et al.*, Mol. Cryst. Liq. Cryst. **398**, 269 (2003).

[15] P. Cicuta, *et al.*, Phys. Rev. E **70**, 011703 (2004).
[16] S. Fan, *et al.*, Phys. Rev. Lett. **80**, 960 (1998).
[17] E. Chow, *et al.*, Opt. Lett. **26**, 286 (2001).
[18] A. Mekis, *et al.*, Phys. Rev. Lett. **77**, 3787 (1996).
[19] S. Rennon, *et al.*, Electron. Lett. **37**, 690 (2001).
[20] R. Slusher and B. Eggleton, *Nonlinear Photonic Crystals* (Springer, Berlin, 2003).
[21] Y. Rostovtsev *et al.*, Phys. Rev. A **57**, 4919 (1998).
[22] Jan Perina, Jr. *et al.*, Phys. Rev. A **70**, 043816 (2004)
[23] D. Petrosyan *et al.*, Phys. Rev. A **64**, 023810 (2001).
[24] G. Kurizki *et al.*, in *Microcavities and Photonic Bandgaps: Physics and Applications*, edited by J. Rarity and C. Weissbuch (Kluwer, London, 1996), p.559.
[25] See, e.g., C. Bowden and A. Zheltikov, J. Opt. Soc. Am. B **19**, 2046 (2002) for a comprehensive review of nonlinear optical effects in photonic crystals.
[26] H. Kosaka *et al.*, Phys. Rev. B **58**, R10096 (1998).
[27] M. Notomi, Phys. Rev. B **62**, 10696 (2000).
[28] X. Zhang, *et al.*, Appl. Phys. Lett. **85**, 341 (2004).
[29] H. Schriemer *et al.*, Phys. Rev. A **63**, 011801(R) (2000).
[30] M. Centini, *et al.*, Phys. Rev. E **67**, 036617 (2003).
[31] M. Singh *et al.*, Phys. Rev. A **69**, 023807 (2004).
[32] X. Wang *et al.*, Phys. Rev. Lett. **93**, 073901 (2004).
[33] M. De Dood *et al.*, Phys. Rev. Lett. **93**, 040504 (2004).
[34] P. Yeh and A. Yariv, *Optical Waves in Layered Media* (Wiley, New York, 1988).
[35] J. D. Jackson, *Classical Electrodynamics*, 2nd ed. (Wiley, New York, 1975).
[36] A. Krokhin *et al.*, Phys. Rev. B **53**, 1205 (1996).
[37] M. Sigalas *et al.*, Phys. Rev. B **49**, 11080 (1994).
[38] M. Sigalas *et al.*, Phys. Rev. B **48**, 14121 (1993).
[39] A. Tip *et al.*, J. Phys. A **33**, 6223 (2000).
[40] Early attempts to create optical lattices are discussed, e.g., in B. Lounis *et al.*, Europhys. Lett. **21**, 13 (1993); M. Weidemuller *et al.*, Europhys. Lett. **27**, 42 (1994); and in G. Grynberg *et al.*, Phys. Rev. Lett. **70**, 2249 (1993).
[41] I. Deutsch *et al.*, Phys. Rev. A **52**, 1394 (1995).
[42] D. van Coevorden *et al.*, Phys. Rev. Lett. **77**, 2412 (1996).
[43] S. Harris, Phys. Today **50**, 36 (1997).
[44] A. Andre *et al.*, Phys. Rev. Lett. **89**, 143602 (2002).
[45] M. Bajcsy *et al.*, Nature (London) **426**, 638 (2003).
[46] Common band-gap modifications require changing of the photonic crystal refractive index over time and schemes have focused primarily on electro and thermo optics band-edge tuning via infiltrated liquid crystals [see, e.g., K. Busch *et al.*, Phys. Rev. Lett. **83**, 967 (1999); D. Kang *et al.*, *ibid.* **86**, 4052 (2001)]. Faster modifications can be attained via nonresonant processes such as Kerr effect or resonant processes in which free electrons and holes are created [see, e.g., M. Gallant *et al.*, Phys. Rev. B **26**, 2133 (1982)].
[47] M. Galli *et al.*, Phys. Rev. B **69**, 115107 (2004).
[48] F. Bassani and G. Pastori Parravicini, *Electronic States and Optical Transitions in Solids* (Pergamon Press, Oxford, 1975).
[49] M. Artoni *et al.*, Phys. Rev. A **63**, 023805 (2001).
[50] M. Artoni *et al.*, Europhys. Lett. **49**, 445 (2000).
[51] S. Chesi *et al.*, Phys. Rev. Lett. **91**, 057402 (2003).
[52] V. Agranovich and V. Ginzburg, *Crystal Optics with Spatial Dispersion and Excitons*, 2nd ed. (Springer, Berlin, 1984).
[53] The absorption profile may also be modified by changing $\mathcal{N}$ in which case higher densities would yield a peak absorption increase along with a linewidth broadening.
[54] Jon M. Bendickson *et al.*, Phys. Rev. E **53**, 4107 (1996).
[55] Jonathan P. Dowling *et al.*, IEEE Journal of Lightwave Technology **17**, 2142 (1999), special issue on Electromagnetic Crystal Structures, Design, Synthesis, and Applications.
[56] M. Born and E. Wolf, *Principles of Optics*, 6th ed. (Cambridge University Press, Cambridge, UK, 1980).
[57] See, e.g., [56], Sec. 1.6.4.
[58] F. Bloch, Z. Phys. **52**, 555 (1928).
[59] William H. Zachariasen, *Theory of X-Ray Diffraction in Crystals* (Dover, New York, 1945), p. 102.
[60] Here the X point denotes as usual the symmetry point of the Brillouin zone for which $k' = \pi/a$, see, e.g. [48].
[61] For our stack of atomic layers such an effective index may well be taken as $\tilde{\eta}(\omega) \simeq \eta(\omega)d + (a-d)/a$.
[62] For a nondispersive nonabsorbing atomic medium the Bragg frequency (ω_B) is typically defined through Eq. (23) where $\tilde{\eta} \approx 1$. One clearly has $\omega_B \simeq (\pi c/a) \times (\omega_o/ck_o) = \omega_o \lambda_o/2a$ so that in Figs. 3 and 5, e.g., ω_B lies, respectively, slightly above or below resonance.
[63] The concept of group velocity would hardly mantain a clear physical significance in the presence of steep absorption. See, e.g., L. Brillouin, in *Wave Propagation and Group Velocity* (Academic, New York, 1960).
[64] M. Artoni *et al.*, Phys. Rev. A **55**, 1347 (1997).
[65] For nanometer scale fluctuations in the layer thickness d, a rough estimate yields an uncertainty over the ratio d/a of the order of 2.5×10^{-3}. Such an uncertainty would only produce, for instance in Fig. 3, a few percents uncertainty in the two gaps position, the overall structure of the band-gap region remaining essentially the same. Any realistic photonic crystal is periodic yet with some imperfections largely due to fluctuations in the position and size of the crystal building blocks. In practice this often becomes a fundamental hindrance in reaching the required fidelity over long ranges; see, e.g., A. F. Koenderink and W. L. Vos, Phys. Rev. Lett. **91**, 213902 (2003).
[66] As a rough estimate for l_{abs} in the resonance region one may take the length at which $e^{-k'' l_{abs}}$ reduces to less than one percent and likewise for l_{ext} in a frequency domain in which absorption is negligible.
[67] M. Raizen *et al.*, Phys. Today **50** (7), 30 (1997).
[68] M. Holthaus, J. Opt. B: Quantum Semiclassical Opt. **2**, 589 (2000).
[69] M. Cristiani *et al.*, Phys. Rev. A **65**, 063612 (2002).
[70] C. Fort, *et al.*, in *Bosons and Fermions in a 1D Optical Lattice, Proceedings of XVI International Conference on Laser Spectroscopy*, edited by P. Hannaford, A. Sidorov, H. Bachor, and K. Baldwin (World Scientific, London, 2004).
[71] A misalignment χ between the two counterpropagating beams, and measured with respect to x along which direction the two beams are perfectly aligned, modifies the lattice spacing as $a \rightarrow a/\sin(\pi/2 - \chi/2)$. The band-gap structure in Fig. 5 results from taking $\chi \simeq 12$ mrad.
[72] L. Pitaeskii and S. Stringari, *Bose-Einstein Condensation* (Clarendon Press, Oxford, 2003).
[73] This is achieved through a large misalignment ($\chi \simeq 150$ mrad) causing an appreciable modification of the atomic lattice periodicity a.